

## Symmetry analysis of self-written waveguides in bulk photosensitive media

L. Poladian,<sup>1</sup> M. Senthilvelan,<sup>1,2</sup> J. A. Besley,<sup>1,2</sup> and C. Martijn de Sterke<sup>2</sup>

<sup>1</sup>*Optical Fibre Technology Centre, The University of Sydney, Australian Technology Park, New South Wales 1430, Australia*

<sup>2</sup>*School of Physics, The University of Sydney, New South Wales 2006, Australia*

(Received 14 August 2003; published 28 January 2004)

The dynamics of self-written waveguides in bulk photosensitive media is studied in detail and contrasted with previous results for planar geometry. We investigate the symmetry and integrability properties of the coupled nonlinear partial differential equations which describe this process. We derive similarity-reduced differential equations and study some of these equations numerically.

DOI: 10.1103/PhysRevE.69.016608

PACS number(s): 42.65.Wi, 02.20.Tw

### I. INTRODUCTION

In recent years, considerable progress has been made in understanding the dynamics of light-induced self-written waveguides both experimentally and theoretically [1–3]. A self-written waveguide is a waveguide that has evolved due to a propagating beam while the beam is in turn guided by the evolving waveguide. For example, consider a beam at normal incidence onto the edge of a uniform, unexposed photosensitive material. The beam initially diffracts in the waveguide, while the maximum intensity over any transverse section remains on the propagation axis. Consequently, the maximum change in the refractive index is along the propagation axis. If the refractive index increases due to exposure, as would be the case for many materials, the modulated profile acts against the diffraction and confines the light more strongly. Over time this can lead to the formation of a narrow channel around the axis, referred to as a self-written waveguide. This waveguide can be used to guide light at other wavelengths as the change in index is long lasting.

Examples of media in which self-writing has been observed include photosensitive glasses [1,4], electro-optic crystals [5] in planar geometries, photoresist [6,7], photopolymerizable resin [8], uv-cured epoxy [9], and bulk silica glass [10]. Similar effects are also observed in photorefractive materials [11]. Recently, the interaction of self-written waveguides has also been studied experimentally and numerically in photopolymerizable resin [12]. Even though a number of studies have been made in planar (slab) materials only few attempts have been made to understand the dynamics in bulk materials. Recently Ljungström and Monro studied the self-writing effects in bulk chalcogenide glass and compared the results with their numerical modeling of this process. They performed the experiments in bulk Nd-doped Bk7 glass (Schott Optical, www.schott.com) [13] and Ce-doped Ga-La-S [14].

Mathematically two equations are used to describe the self-writing process. One is the paraxial wave equation describing the propagation of light through the material:

$$ik_0 n_0 \frac{\partial \mathcal{E}}{\partial z} + \frac{1}{2} \left( \frac{\partial^2}{\partial x^2} + \frac{\partial^2}{\partial y^2} \right) \mathcal{E} + k_0^2 n_0 \Delta n \mathcal{E} = 0, \quad (1)$$

where  $\mathcal{E}$  is the electric field amplitude,  $n_0$  is the initial refractive index,  $k_0 = 2\pi/\lambda$  is the wave number in the unexposed

materials, and  $\Delta n$  is the refractive index change. The first term in Eq. (1) describes propagation, the second diffraction, and the third accounts for how photosensitive refractive index changes affect light propagation. Only the diffraction term differs from that considered in Ref. [15] due to the extra transverse dimension.

The second equation describes the refractive index evolution. The most general form we consider here is

$$\frac{\partial \Delta n}{\partial t} = F(|\mathcal{E}|, \Delta n), \quad (2)$$

where  $F$  is a function describing how the rate of change of the refractive index depends on the intensity and local refractive index.

For the remainder of the paper we work with Eqs. (1) and (2) in dimensionless form, by defining

$$T = a_0^2 k_0^2 n_0 F_0 t, \quad (3a)$$

$$X = x/a_0, \quad (3b)$$

$$Y = y/a_0, \quad (3c)$$

$$Z = z/(k_0 n_0 a_0^2), \quad (3d)$$

$$\mathcal{F} = \mathcal{E}/F_0, \quad (3e)$$

$$N = a_0^2 k_0^2 n_0 \Delta n, \quad (3f)$$

$$E = \mathcal{E}/\mathcal{E}_0. \quad (3g)$$

Here  $a_0$  is a characteristic measure of the beam width,  $\mathcal{E}_0$  is a characteristic electric field amplitude, and  $F_0 = F(|\mathcal{E}_0|, 0)$ . The normalized equations are thus

$$iE_Z + \nabla_{\perp}^2 E + NE = 0, \quad (4a)$$

$$N_T - \mathcal{F}(|E|, N) = 0, \quad (4b)$$

where the transverse Laplacian is given by

$$\nabla_{\perp}^2 = \frac{\partial^2}{\partial X^2} + \frac{\partial^2}{\partial Y^2} \quad (5a)$$

$$= \frac{\partial^2}{\partial R^2} + \frac{1}{R} \frac{\partial}{\partial R} + \frac{1}{R^2} \frac{\partial^2}{\partial \Theta^2} \quad (5b)$$

in Cartesian and cylindrical coordinates, respectively, with  $X=R \cos \Theta$  and  $Y=R \sin \Theta$ .

An important special case that we consider in detail is the power law

$$F(|\mathcal{E}|, \Delta n) = F(|\mathcal{E}|) = A |\mathcal{E}|^{2p}, \quad (6)$$

where  $A$  is a constant describing the strength of the photosensitivity and  $p$  is the number of photons involved in the process. For example, for a one-photon process we have  $p=1$  while for a two-photon process  $p=2$ . In the normalized system of equations, this function becomes

$$\mathcal{F} = |E|^{2p}. \quad (7)$$

All results and figures in this paper are in terms of the dimensionless quantities defined in Eqs. (3).

In this paper we explore the mathematical properties of the system of nonlinear partial differential equations (PDEs) (4) in detail. To date, theoretical studies of the self-writing process in bulk geometry have been limited to numerical simulations [4,14]. Using Painlevé analysis [16,17] it has been shown that the equations for self-writing in planar geometry are nonintegrable [15] for the case of a power-law photosensitivity with  $p=1$  or  $p=2$ . We have found that the equations for bulk geometry are also nonintegrable with this photosensitivity. Since the calculations are virtually identical to the planar case we do not reprint them here. In order to construct some exact and physically interesting solutions for this problem we use Lie group analysis [18,19], which is one of the powerful methods to extract exact solutions for nonlinear PDEs. It is noted that similarity methods have been applied to Hill gratings [20], stimulated Raman scattering [21], and parabolic pulses in optical fibers [22].

The paper is organized as follows. In Sec. II, we present Lie symmetry analysis for these equations, discuss the physical interpretation of the various symmetries uncovered, and use these to construct similarity-reduced PDE involving fewer independent variables. In Sec. III, we reduce the equations further to obtain a system of ordinary differential equations (ODEs) for which we find a class of self-similar modal solutions. This is the first class of solutions presented for self-writing in a bulk material. In Sec. IV we present numerical analyses of both the full set of nonlinear PDEs presented above, and also of a particular reduced set of equations. The numerical solutions are found to converge to the self-similar solution for a wide range of initial conditions, suggesting that the self-similar solution is physically significant. Finally, we give our conclusions in Sec. V.

In Appendix A we present numerical results for the planar case that complement previous studies. In Appendix B we show an alternative special case of the similarity reductions which, while having some interesting mathematical properties, does not lead to physically interesting predictions. Finally, we discuss alternative similarity variables in Appendix C.

## II. LIE SYMMETRY ANALYSIS

We start with the generic form of the self-writing equations (4) and introduce the transformation to the real functions corresponding to amplitude and phase,

$$E = \mathcal{A}(X, Y, Z, T) e^{i\Phi(X, Y, Z, T)}, \quad (8)$$

so that they can be written as

$$\mathcal{A}_Z + \frac{1}{2} \mathcal{A} \nabla_{\perp}^2 \Phi + \mathcal{A}_X \Phi_X + \mathcal{A}_Y \Phi_Y = 0, \quad (9a)$$

$$- \mathcal{A} \Phi_Z + \frac{1}{2} \nabla_{\perp}^2 \mathcal{A} - \frac{1}{2} \{ \Phi_X^2 + \Phi_Y^2 \} \mathcal{A} + N \mathcal{A} = 0, \quad (9b)$$

$$N_T - \mathcal{F}(\mathcal{A}, N) = 0. \quad (9c)$$

Let us consider a one-parameter Lie group of infinitesimal transformations,

$$X \rightarrow X + \varepsilon \xi^{(X)}(X, Y, Z, T, \mathcal{A}, \Phi, N), \quad (10)$$

where  $\varepsilon \ll 1$ . Analogous transformations are defined for the remaining dependent and independent variables. The associated vector field is

$$V = \xi^{(X)} \frac{\partial}{\partial X} + \xi^{(Y)} \frac{\partial}{\partial Y} + \xi^{(Z)} \frac{\partial}{\partial Z} + \xi^{(T)} \frac{\partial}{\partial T} + \xi^{(\mathcal{A})} \frac{\partial}{\partial \mathcal{A}} + \xi^{(\Phi)} \frac{\partial}{\partial \Phi} + \xi^{(N)} \frac{\partial}{\partial N}. \quad (11)$$

The invariance of Eqs. (9) under the infinitesimal point transformations (10) leads to the invariance condition

$$\text{Pr}^{(2)} V(\Delta) \Big|_{\Delta=0} = 0, \quad (12)$$

where  $\text{Pr}^{(2)} V$  is the second prolongation of the vector field (11) [18,19]. The solution of the resulting determining equations arising from Eq. (12) yields the infinitesimals. The presence of free parameters and arbitrary functions determines the number and type of different symmetries the equations possess. We have used the computer programs MUMATH [23] and MATHLIE [24] to determine the symmetries. Symmetries associated with finite dimensional subspaces are indicated with a capital letter, and infinite dimensional symmetry groups associated with arbitrary functions are denoted by a lowercase letter.

The most general photosensitivity equations support eight symmetries and the associated vector field (11) can be written as

$$V = a V_X + b V_Y + c V_Z + d V_T + e V_{\Theta} + f V_U + g V_V + V_{\phi}(h), \quad (13)$$

where the first four symmetries correspond to the homogeneity of the spatial and temporal coordinates

$$V_X = \frac{\partial}{\partial X}, \quad V_Y = \frac{\partial}{\partial Y}, \quad (14a)$$

$$V_Z = \frac{\partial}{\partial Z}, \quad (14b)$$

$$V_T = \frac{\partial}{\partial T}. \quad (14c)$$

The next three symmetries correspond to the isotropy of the system and how it behaves under coordinate rotations:

$$V_\Theta = X \frac{\partial}{\partial Y} - Y \frac{\partial}{\partial X} = \frac{\partial}{\partial \Theta}, \quad (14d)$$

$$V_U = Z \frac{\partial}{\partial X} + X \frac{\partial}{\partial \Phi}, \quad V_V = Z \frac{\partial}{\partial Y} + Y \frac{\partial}{\partial \Phi}. \quad (14e)$$

The first symmetry above is a simple rotation about the axis of propagation. The next two symmetries correspond to tilting the axis of propagation and simultaneously adding a linear phase variation to the wave front. The paraxial approximation to the wave equation has modified these symmetries from the pure isotropic case.

The last symmetry is an infinite dimensional symmetry (since it contains an arbitrary function) and corresponds to adding an arbitrary function of time to the phase of the field:

$$V_\phi(h) = h(T) \frac{\partial}{\partial \Phi}. \quad (14f)$$

The planar results can be easily obtained from the above analysis by discarding any symmetries that included the unwanted Cartesian coordinate.

### A. Nonsaturating systems

We now assume that the photosensitive growth law  $F$  does not depend on the refractive index distribution, i.e.,  $\mathcal{F} = \mathcal{F}(\mathcal{E})$ . This implies that the changes do not depend on the current value of the index, which precludes effects such as saturation. However, all real physical systems exhibit some form of saturation that prevents the refractive index  $N$  changing without bound. The maximum value of  $N$  achievable depends both on the writing conditions and the material. An analysis of the effect of saturation on the evolution of self-written systems [2] suggests saturation values as large as  $N \sim 160$  for photopolymers but only  $N \sim 15$  for typical photosensitive glasses. Nevertheless, the nonsaturating approximation is a physical model under a variety of situations and provides useful understanding of the system even in cases where it is not perfectly accurate. In addition, it is a good model for the initial evolution of a photosensitive system, since the effect of saturation is then weak.

When  $\mathcal{F} = \mathcal{F}(\mathcal{E})$  two new symmetries emerge:

$$V_S = Z \frac{\partial}{\partial Z} + \frac{1}{2} \left\{ X \frac{\partial}{\partial X} + Y \frac{\partial}{\partial Y} \right\} - T \frac{\partial}{\partial T} - N \frac{\partial}{\partial N}, \quad (15a)$$

$$V_\psi(l) = l(Z) \frac{\partial}{\partial \Phi} + l'(Z) \frac{\partial}{\partial N}. \quad (15b)$$

The first is a scaling symmetry. The second symmetry allows an arbitrary function of  $Z$  to be added to the phase, provided its derivative is added to the index profile.

### B. Power-law photosensitive growth

We now further specialize to

$$\mathcal{F}(|E|) = |E|^{2p}, \quad (16)$$

where  $p$  is arbitrary. Three new infinite dimensional symmetries arise:

$$V_x(u) = u(Z) \frac{\partial}{\partial X} + u'(Z) X \frac{\partial}{\partial \Phi} + u''(Z) X \frac{\partial}{\partial N}, \quad (17a)$$

$$V_y(v) = v(Z) \frac{\partial}{\partial Y} + v'(Z) Y \frac{\partial}{\partial \Phi} + v''(Z) Y \frac{\partial}{\partial N}, \quad (17b)$$

$$V_t(g) = g(T) \frac{\partial}{\partial T} - \frac{1}{2p} \dot{g}(T) \mathcal{A} \frac{\partial}{\partial \mathcal{A}}. \quad (17c)$$

The first pair of symmetries corresponds to arbitrary stretching of the transverse coordinates accompanied by corresponding changes to the phase and index. They contain as special cases the pure translation (14a) and tilt (14e) symmetries when the arbitrary functions are chosen to be constant or linear, respectively. The last symmetry corresponds to arbitrary stretching of time with related scaling of the field amplitude. It contains the time translation symmetry as a special case when the arbitrary function is taken to be constant. When  $g(T) = T$  this last symmetry can be combined with the scaling symmetry to yield an alternative scaling symmetry,

$$V_{S'} = Z \frac{\partial}{\partial Z} + \frac{1}{2} \left\{ X \frac{\partial}{\partial X} + Y \frac{\partial}{\partial Y} \right\} - \frac{1}{2p} \mathcal{A} \frac{\partial}{\partial \mathcal{A}} - N \frac{\partial}{\partial N}. \quad (18)$$

This symmetry is more convenient to work with in the power-law case because it commutes with  $V_t(g)$ .

### C. Special symmetries

The power-law equations support a further symmetry which only occurs for specific values of the parameter  $p$ :

$$V_z(f) = f(Z) \frac{\partial}{\partial Z} + \frac{R^2}{4} \left\{ f''(Z) \frac{\partial}{\partial \Phi} + f'''(Z) \frac{\partial}{\partial N} \right\} + \frac{f'(Z)}{2} \left\{ X \frac{\partial}{\partial X} + Y \frac{\partial}{\partial Y} - \frac{1}{p} \mathcal{A} \frac{\partial}{\partial \mathcal{A}} - 2N \frac{\partial}{\partial N} \right\}. \quad (19)$$

This symmetry contains  $V_Z$  and  $V_{S'}$  as special cases when the arbitrary function is taken as constant and linear, respectively. The above symmetry emerges from Eq. (12) with the condition

$$(Dp - 2) \mathcal{A} f''(Z) = 0, \quad (20)$$

where  $D$  is the transverse dimensionality. Thus the special values of  $p = 2/D$  emerge from the prolongation, and the two special cases of the symmetry that satisfy  $f''(Z) = 0$  are

present for all values of  $p$ . In the planar case the special symmetry exists when  $p=2$ , in the bulk case it exists when  $p=1$ .

#### D. Commutators

The nonzero commutators between these symmetry operators reveal how the symmetries can be exploited. Commuting symmetries can be exploited serially, because using one to reduce the order of the equation leaves the other symmetry intact. If the symmetries do not commute, then they must either be exploited together or one symmetry must be abandoned. For example, exploiting rotational symmetry requires abandoning transverse translational symmetry and vice versa. Even exploiting noncommuting symmetries simultaneously usually leads to uninteresting results. For example, fields which are simultaneously rotationally *and* translationally symmetric are not very interesting (they tend to be constant and thus not localized). The nonzero commutators for the most general symmetries are given below. The commutators for the special cases can be extracted directly from the general cases:

$$[V_x(u_1), V_x(u_2)] = V_\psi(u_1 u_2' - u_1' u_2), \quad (21a)$$

$$[V_y(v_1), V_y(v_2)] = V_\psi(v_1 v_2' - v_1' v_2), \quad (21b)$$

$$[V_z(f_1), V_z(f_2)] = V_z(f_1 f_2' - f_1' f_2), \quad (21c)$$

$$[V_i(g_1), V_i(g_2)] = V_i(g_1 \dot{g}_2 - \dot{g}_1 g_2), \quad (21d)$$

$$[V_x(u), V_\Theta] = V_y(u), \quad (21e)$$

$$[V_y(v), V_\Theta] = -V_x(v), \quad (21f)$$

$$[V_x(u), V_z(f)] = V_x(\frac{1}{2} u f' - u' f), \quad (21g)$$

$$[V_y(v), V_z(f)] = V_y(\frac{1}{2} v f' - v' f), \quad (21h)$$

$$[V_i(g), V_\phi(h)] = V_\phi(g h'), \quad (21i)$$

$$[V_z(f), V_\psi(l)] = V_\psi(l' f). \quad (21j)$$

#### E. Reduced system

Similarity variables can be obtained by solving the invariant surface condition given by the equations

$$\frac{dX}{\xi^{(X)}} = \frac{dY}{\xi^{(Y)}} = \frac{dZ}{\xi^{(Z)}} = \frac{dT}{\xi^{(T)}} = \frac{dA}{\xi^{(A)}} = \frac{d\Phi}{\xi^{(\Phi)}} = \frac{dN}{\xi^{(N)}}. \quad (22)$$

These equations are difficult to solve in complete generality, and moreover would yield expressions difficult to interpret physically. Thus, by carefully examining the commutator structure and the physical meaning of the various symmetries we explore a particular subset of symmetries and similarity variables.

We defer discussion of the special symmetries (19) to Appendix B. The symmetries associated with adding func-

tions of  $T$  and  $Z$  to the phase of the field do not yield interesting physics and are also discussed in Appendix B. We also choose not to exploit any symmetry that destroys the symmetry in  $\Theta$ . Thus we retain the subgroup spanned by the symmetries  $V = V_i(g) + V_z(f)$  with  $f(Z) = 2s(Z - Z_0)$  restricted to a linear function of  $Z$  as a consequence of Eq. (20). The relevant invariant surface condition is then

$$\begin{aligned} \frac{dX}{sX} &= \frac{dY}{sY} = \frac{dZ}{2s(Z - Z_0)} = \frac{dT}{g(T)} \\ &= -\frac{2p dA}{(\dot{g}(T) + 2s)\mathcal{A}} = \frac{d\Phi}{0} = -\frac{dN}{2sN}. \end{aligned} \quad (23)$$

We see that we can take  $s=1$  without loss of generality.

Solving for a similarity variable gives

$$\tilde{X} = \phi(T)X, \quad (24a)$$

$$\tilde{Y} = \phi(T)Y, \quad (24b)$$

$$\tilde{Z} = \phi(T)^2(Z - Z_0), \quad (24c)$$

with the dependent variables scaling as

$$\tilde{\mathcal{A}}(\tilde{X}, \tilde{Y}, \tilde{Z}) = \left( \frac{\sqrt{g(T)}}{\phi(T)} \right)^{1/p} \mathcal{A}(X, Y, Z, T), \quad (24d)$$

$$\tilde{\Phi}(\tilde{X}, \tilde{Y}, \tilde{Z}) = \Phi(X, Y, Z, T), \quad (24e)$$

$$\tilde{N}(\tilde{X}, \tilde{Y}, \tilde{Z}) = \frac{1}{\phi^2(T)} N(X, Y, Z, T), \quad (24f)$$

where

$$\phi(T) = \exp\left( \int^T \frac{dT'}{g(T')} \right), \quad (25)$$

or equivalently

$$g(T) = \frac{\phi(T)}{\dot{\phi}(T)}. \quad (26)$$

The reduced PDEs are

$$i\tilde{E}_{\tilde{z}} + \frac{1}{2}\tilde{\nabla}_{\tilde{z}}^2 \tilde{E} + \tilde{N}\tilde{E} = 0, \quad (27a)$$

$$2\tilde{N} + \tilde{X}\tilde{N}_{\tilde{x}} + \tilde{Y}\tilde{N}_{\tilde{y}} + 2\tilde{Z}\tilde{N}_{\tilde{z}} - |\tilde{E}|^{2p} = 0. \quad (27b)$$

Note that

$$\tilde{R}\tilde{N}_{\tilde{r}} = \tilde{X}\tilde{N}_{\tilde{x}} + \tilde{Y}\tilde{N}_{\tilde{y}} \quad (28)$$

in cylindrical coordinates and thus the angular dependence never explicitly appears in the photosensitivity equation. Equations (27) are investigated numerically in Sec. IV.

**F. Scaling laws**

Before we study the system further we discuss the physical significance of the transformations. The arbitrary function  $\phi(T)$  produces a scaling of the transverse coordinates. While the transverse coordinates shrink, the longitudinal coordinate shrinks as the square of  $\phi(T)$  and the height of the refractive index profile grows correspondingly. The amplitude of the field profile also grows but with a different dependence on  $\phi(T)$ . This is precisely the kind of behavior seen in experiments and numerical simulations once a waveguiding structure has formed.

Experiments and numerical simulations have a constant input field, usually with a Gaussian profile. Although it is not possible to introduce this condition into the above solution, the total power can be required to be constant. Imposing this condition leads to a specific form for the previously arbitrary function  $\phi(T)$ .

The total power in the original and reduced systems can be written as, respectively,

$$\mathcal{P} = \int |E|^2 dA, \tag{29a}$$

$$\tilde{\mathcal{P}} = \int |\tilde{E}|^2 d\tilde{A}, \tag{29b}$$

where in both cases the integration is over the complete transverse cross section. Note that  $\tilde{\mathcal{P}}$  is a pure constant. Comparing the two power expressions yields

$$\frac{\mathcal{P}}{\tilde{\mathcal{P}}} = \left( \frac{\phi(T)^2}{g(T)} \right)^{1/p} \frac{1}{\phi(T)^D}, \tag{30}$$

where  $D$  is again the transverse dimensionality of the system. Rearranging Eq. (30) and requiring the total power in the original system to be independent of  $T$  yield the differential equation

$$\frac{\partial \phi}{\partial T} = \left( \frac{\mathcal{P}}{\tilde{\mathcal{P}}} \right)^p \phi^{Dp-1}, \tag{31}$$

generalizing earlier work by Monro *et al.* [25]. When  $p \neq 2/D$  the scaling has a power-law behavior

$$\phi(T) = \left\{ (2-Dp) \left( \frac{\mathcal{P}}{\tilde{\mathcal{P}}} \right)^p (T-T_i) \right\}^{1/(2-Dp)}, \tag{32}$$

where  $T_i$  is a constant of integration. In the special case  $p = 2/D$  the scaling law becomes exponential,

$$\phi(T) = \exp \left\{ \left( \frac{\mathcal{P}}{\tilde{\mathcal{P}}} \right)^p (T-T_i) \right\}. \tag{33}$$

We make the following general observations. The scaling function  $\phi(T)$  is always monotonically increasing. It reaches a singularity within a finite time  $T_i$  when  $Dp > 2$ . In a planar

geometry, this would occur for a three-photon process, but in a bulk geometry a singularity occurs for the two-photon process.

**G. Secondary Lie analysis**

The reduced PDEs (27) in three independent variables can be further analyzed for symmetry properties by repeating the Lie analysis. We represent the vector fields using tildes to distinguish them from the vector fields obtained in the first-level analysis. The analysis uncovers a three-dimensional subspace of symmetries:

$$\tilde{V}_\Theta = \tilde{X} \frac{\partial}{\partial \tilde{Y}} - \tilde{Y} \frac{\partial}{\partial \tilde{X}} = \frac{\partial}{\partial \tilde{\Theta}}, \tag{34a}$$

$$\tilde{V}_\Phi = \frac{\partial}{\partial \tilde{\Phi}}, \tag{34b}$$

$$\tilde{V}_N = \log \tilde{Z} \frac{\partial}{\partial \tilde{\Phi}} + \frac{1}{\tilde{Z}} \frac{\partial}{\partial \tilde{N}}, \tag{34c}$$

and one more symmetry which only exists when  $D=1$ ,

$$\tilde{V}_X = \sqrt{\tilde{Z}} \frac{\partial}{\partial X} + \frac{X}{2\sqrt{\tilde{Z}}} \frac{\partial}{\partial \tilde{\Phi}} - \frac{X}{4\tilde{Z}^{3/2}} \frac{\partial}{\partial \tilde{N}}. \tag{34d}$$

We have not discovered any physically appealing similarity reductions using these symmetries, apart from the restriction to a circularly symmetric solution, which we discuss in Appendix B.

**III. SELF-SIMILAR MODAL SOLUTIONS**

In this section we restrict our attention to the bulk geometry since the planar case has been dealt with previously [25]. Our aim is to explain mathematically some of the features observed in experiments and numerical simulations. A careful investigation shows that when the self-written waveguide evolves, its shape appears to remain approximately constant even though its depth and width change. A modal solution has the properties that the waveguide and the intensity profile are independent of  $\tilde{Z}$ , and that the phase is independent of any transverse coordinates and linear in  $\tilde{Z}$ . Without loss of generality we take  $\tilde{\Phi} = \tilde{Z}$ . Furthermore, we only consider cylindrically symmetrical modes. Inserting these assumptions into the PDE from the preceding section yields the ODE

$$\frac{1}{2} \left( \tilde{\mathcal{A}}'' + \frac{1}{\tilde{R}} \tilde{\mathcal{A}}' \right) + (\tilde{N} - 1) \tilde{\mathcal{A}} = 0, \tag{35a}$$

$$2\tilde{N} + \tilde{R} \tilde{N}' - \tilde{\mathcal{A}}^{2p} = 0, \tag{35b}$$

where the prime indicates differentiation with respect to the only remaining independent variable  $\tilde{R}$ .

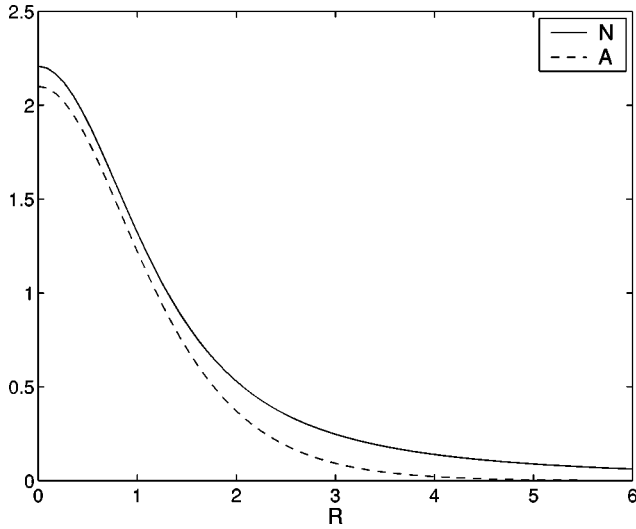


FIG. 1. Self-similar solutions of the self-writing problem for one-photon process. The dashed and solid lines represent the shapes of the field mode  $\tilde{A}$  and the refractive index profile  $\tilde{N}$ , respectively. All quantities in this and subsequent figures are in dimensionless units.

To summarize, we used the following transformation to transform Eq. (4) to an ODE (35):

$$E(R, \Theta, Z, T) = \sqrt{\frac{\tilde{\mathcal{P}}}{\tilde{\rho}}} \phi(T) \tilde{A}(\tilde{R}) e^{i\phi(T)^2 Z}, \quad (36a)$$

$$N(R, \Theta, Z, T) = \phi(T)^2 \tilde{N}(\tilde{R}). \quad (36b)$$

In this form we can identify the propagation constant in terms of the scaling law:

$$\beta(T) = \phi(T)^2. \quad (37)$$

#### Modal and index profiles

Solving Eqs. (35) we can find the shapes of the mode and refractive index. We use a one-dimensional shooting method to solve these coupled system of ODEs. We search for a value of  $\tilde{A}(0)$  that gives a solution which vanishes at large  $\tilde{R}$  and has finite power  $\tilde{\mathcal{P}}$ . The value of  $\tilde{N}(0)$  follows automatically from  $\tilde{A}(0)$  through Eq. (36b). We use MATHEMATICA [26] to do so and solutions for the one- and two-photon photosensitivity processes are shown in Figs. 1 and 2, respectively. The modal power  $\tilde{\mathcal{P}}$  in these reduced systems is found by squaring and integrating the transverse shapes  $\tilde{A}(\tilde{R})$ . For the one- and two-photon processes we find  $\tilde{\mathcal{P}} = 14.0517$  and  $4.52772$ , respectively.

If we map the self-similar waveguide back to the original coordinates, we find that it displays some unusual linear guidance properties. It has previously been shown for the planar case that the index profile in the tails decays as  $R^{-2}$  [2], and it can be seen from Eqs. (35) that this is the case for bulk geometry also. We define the  $V$  value of a fiber geometry waveguide as follows:

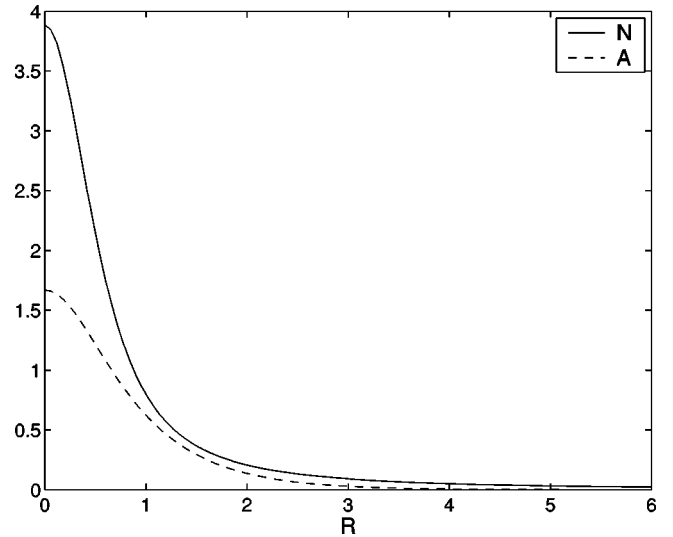


FIG. 2. As Fig. 1, but for  $p=2$ .

$$V = \int_0^\infty dR \sqrt{N}. \quad (38)$$

Given the asymptotic form of the index modulation, it is seen that the waveguide has an infinite  $V$  value, and according to WKB theory would guide an infinite number of discrete guided modes [27]. We have studied a number of these modes and found that they display unusual behavior. Starting from the fundamental mode, the modal profile of successive guided modes are decreasingly well confined, while their propagation constants are closer together and tend toward a constant. This contrasts with a simple index profile, such as a step index waveguide, for which the modal fields have roughly similar levels of confinement, and the separation between propagation constants of successive modes increases [27].

These results are useful for understanding the properties of a self-written waveguide that follows a self-similar evolution. From the perspective of the fundamental mode, all other guided modes are poorly confined and have near identical propagation constants. One would therefore expect to observe behavior consistent with a single-mode waveguide rather than a multimode structure. This would allow an effectively single-moded waveguide to be written relatively easily.

Previous work in this area has noted a beating process in a numerical analysis of the growth of a self-written waveguide in the planar geometry [2]. We can see from the distribution of the effective indices of guided modes that the beat lengths would be practically identical for beating with any one of the other guided modes and also for the lowest order radiation modes.

## IV. NUMERICAL ANALYSIS OF FULL AND REDUCED SYSTEMS

### A. Numerical confirmation of self-similar evolution

The study of photosensitive materials can help understand the growth dynamics of self-written optical waveguides. The

self-similar solution derived above describes the evolution of a waveguide from an initial condition that can be appropriately rescaled in magnitude and in the transverse dimensions to match the index modulation profile defined by the self-similar solution itself, and which is independent of the longitudinal dimension  $Z$ . The input field must also continuously scale with the solution over time, starting from the same scaling factor as the initial index modulation profile. This is clearly a severely limiting set of conditions.

We are ultimately interested in the formation of a waveguide from an initially unexposed, uniform photosensitive waveguide under illumination by a constant source. In this system it would be particularly interesting to investigate whether one can observe the stable formation of a waveguide and if so, how the evolution and features of the waveguide compare with the self-similar solution obtained above. Such analysis must be carried out numerically by integrating Eqs. (4). We implemented a finite-difference scheme to do this. For efficiency reasons, we have expressed Eqs. (4) in cylindrical coordinates and assumed an azimuthally symmetric input condition, and therefore also azimuthally symmetric solutions. The simulation is therefore no more computationally intensive for the bulk geometry than for the planar case.

Studies of planar materials have revealed the remarkable result that after an initial response period, the growth dynamics of a self-written waveguide tend towards those of the self-similar evolution to a high level of accuracy for  $p=1$  and 2 [25]. We have carried out a similar analysis in the bulk geometry case.

The equations describing the self-writing system have been analyzed for a normalized domain of radius 20 and length 4. An input condition of a Gaussian beam with width 1 unit at  $1/e$  field strength was used and the simulation was conducted over a time period of up to 40 units. The index profile was monitored at  $Z=2$  and  $Z=4$  (i.e., midpoint and end face of the simulation). The data were analyzed by comparing profiles with the self-similar solution at each point in time. The evolution of the peak value and the width of the profile are obtained at given times  $T$  and positions  $Z$ , and these converted into scaling factors by dividing by the appropriate quantities for the self-similar solution. A simple numerical estimate of the width was obtained by taking the point at which the index change drops to half of its peak value.

We denote the two scaling factor quantities obtained in this way as  $S_{max}$  and  $S_\rho$ , where the subscripts  $max$  and  $\rho$  refer to the maximum value and the width, respectively. According to the self-similar solution, the evolution of these scaling factors should be related to a single function  $\phi(T)$ , whose form is related to the parameter  $p$ , and the ratio  $\mathcal{P}/\tilde{\mathcal{P}}$ . Specifically, the scaling factors should evolve with time as follows:

$$\begin{aligned} S_{max} &= \phi(T)^2, \\ S_\rho &= 1/\phi(T). \end{aligned} \quad (39)$$

The analysis of a given numerical system should yield these

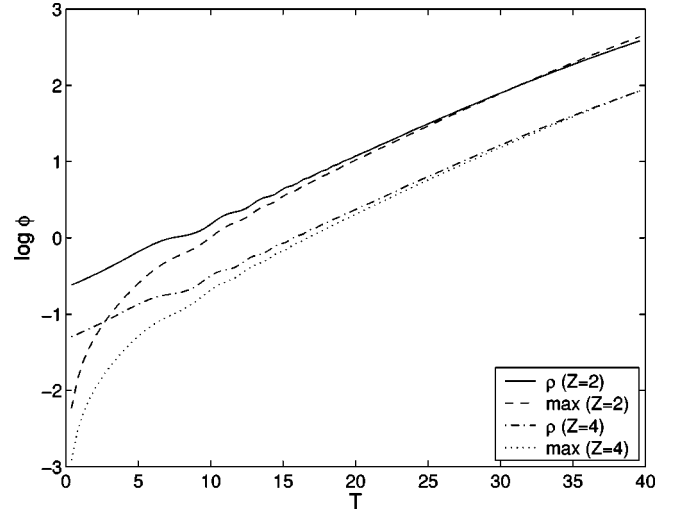


FIG. 3. Variation of the natural logarithm of numerically obtained transformed scaling factors vs time for  $p=1$  and at  $Z=2$  and 4 along the propagation axis.

scaling factors, which can be transformed to estimates of the scaling function, denoted by  $\phi_{max}(T)$  and  $\phi_\rho(T)$ , respectively.

The power  $\mathcal{P}$  can be estimated directly by integrating the intensity within the simulation. It should be noted that the total power within the numerical domain is constant and defined by the excitation condition at  $Z=0$ . This is because we have used a zero field boundary condition and there is no absorption in the simulation. On the other hand, it is possible to estimate the power contained within the waveguiding region by limiting the integration domain. We choose the integration limits according to the width of the index modulation region,  $\rho_N$ , as

$$\mathcal{P} \approx \int_0^{3\rho_N} 2\pi R dR |E(R)|^2. \quad (40)$$

We analyze the numerical data in terms of these measures of the scaling function and power for  $p=1$  and  $p=2$ , respectively. It is noted that the self-written waveguide at all times in these simulations has a finite  $V$  value, as opposed to the fully self-similar solution which has an infinite  $V$  value (Sec. III).

### 1. Numerical analysis— $p=1$

For  $p=1$ , the scaling function  $\phi(T)$  of the self-similar solution grows exponentially with time according to Eq. (33). If the numerical system behaves analogously, then a logarithmic plot of each of the numerically inferred scaling factors  $\phi_{max}(T)$  and  $\phi_\rho(T)$  with time should follow a straight line. Natural logarithms are used throughout this paper. The gradient of this line should be the power ratio  $\mathcal{P}/\tilde{\mathcal{P}}$ , where the reduced modal power was given above as  $\tilde{\mathcal{P}} = 14.0517$ . Figure 3 shows such a plot. The behavior seems to match that predicted in the self-similar solution well at both the midpoint and end face of the simulation. The lines converge well around  $T \approx 14$  and follow a fairly straight line,

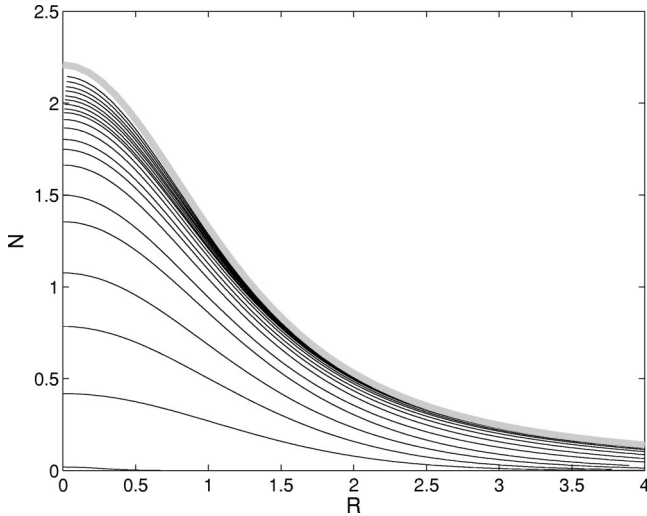


FIG. 4. Evolution of the refractive index with time normalized to a profile of constant width for  $p=1$  at  $Z=4$ . Starting from  $T=0$ , the zero line, subsequent times at intervals of 2 units are characterized by an increasing index at the origin. The thick line indicates the self-similar solution.

with a gradient of roughly 0.085. The straightness of the lines is remarkable given that the scaling factor varies by a factor of about 30 within this plot. We estimate the power using Eq. (40), and obtain the value 1.33, which leads to a gradient of  $1.33/14.0517=0.094$ . This power ratio is consistent with the gradient of the lines given above.

We next observe the evolution of the index with time at the end face. This illustrates the growth of the solution towards a self-similar form. To demonstrate the evolution, we normalized the profile at each time to a constant width given by that of the self-similar solution. The strength of the index profile is normalized by the inverse square root of the scaling used on the width, to be consistent with the self-similar solution. We lay the plots at different times on the same graph, shown in Fig. 4 from  $T=0$  to  $T=40$  at intervals of 2 units. Successive curves converge upwards towards the self-similar solution.

## 2. Numerical analysis— $p=2$

For  $p=2$ , the scaling function  $\phi(T)$  of the self-similar solution evolves according to Eq. (32). In contrast to the  $p=1$  case, this solution collapses in finite time. Figure 5 shows the variation in the transformed scaling factors inferred from numerical analysis of the system for  $p=2$  with time at the midpoint and end point of the simulation. We no longer observe convergence of the curves, however there is clearly an abrupt change in the system around  $T \approx 7$ , at which point the scaling factors for the index modulation grow rapidly and the scaling factors for the field profile fluctuate wildly. This would appear to be the numerical representation of the collapse of the self-similar solution.

The lack of convergence of the curves prior to the collapse could be caused by the fact that the collapse occurs at a relatively early time—in the  $p=1$  case, convergence is not observed until much later.

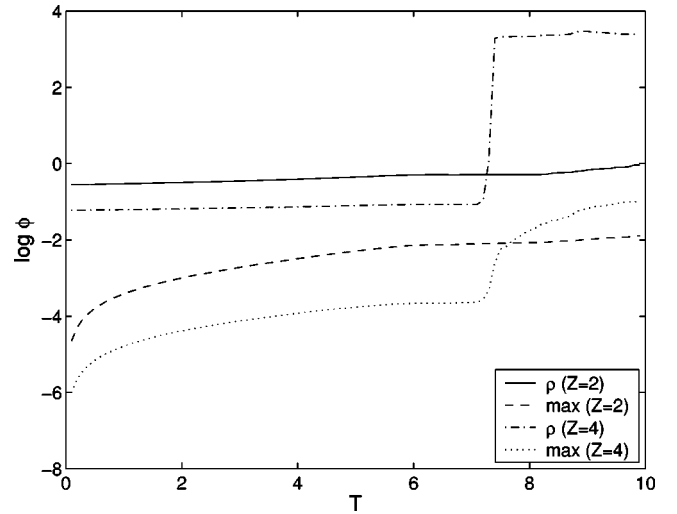


FIG. 5. Plot of variation of the numerically obtained scaling factors as a function of time for  $p=2$  and at  $Z=2$  and 4.

## B. Numerical analysis of reduced system of equations

The self-similar solution is essentially a mode of the reduced system of PDEs (27), so that its stability can be studied through numerical simulations of this system. It is noted, however, that the self-similar solution presented in Sec. III is one of a family of modes that can be obtained depending on the choice of the propagation constant in Eq. (36a). These modes are simply scaled relative to one another, and can be obtained from the self-similar solution in Sec. III by the substitutions

$$\tilde{N} \rightarrow m\tilde{N}, \quad (41a)$$

$$\tilde{\mathcal{A}} \rightarrow m^{1/2p}\tilde{\mathcal{A}}, \quad (41b)$$

$$\tilde{R} \rightarrow \tilde{R}/\sqrt{m}, \quad (41c)$$

where the propagation constant of the scaled solution is simply  $m\phi(T)^2$ . We now present the results of numerical simulations of Eqs. (27), and look for convergence of the field and index modulation terms toward such a scaled self-similar solution.

Our simulations have been obtained using a pair of finite difference schemes representing each of Eqs. (27). For each propagation step, we iterate over both schemes to obtain a solution to both PDEs simultaneously. To confirm the stability and accuracy of this method we checked that the self-similar solution presented in Sec. III propagates as a guided mode of the system. We then conducted simulations for which the initial conditions differ from the self-similar solution.

### 1. Fiber geometry— $p=1$

We consider an initial condition given by the self-similar field solution in combination with a zero index modulation. Figure 6 shows a contour plot of the results of such a simulation for the fiber geometry with  $p=1$ . It suggests the convergence of the solution toward some mode. We compare

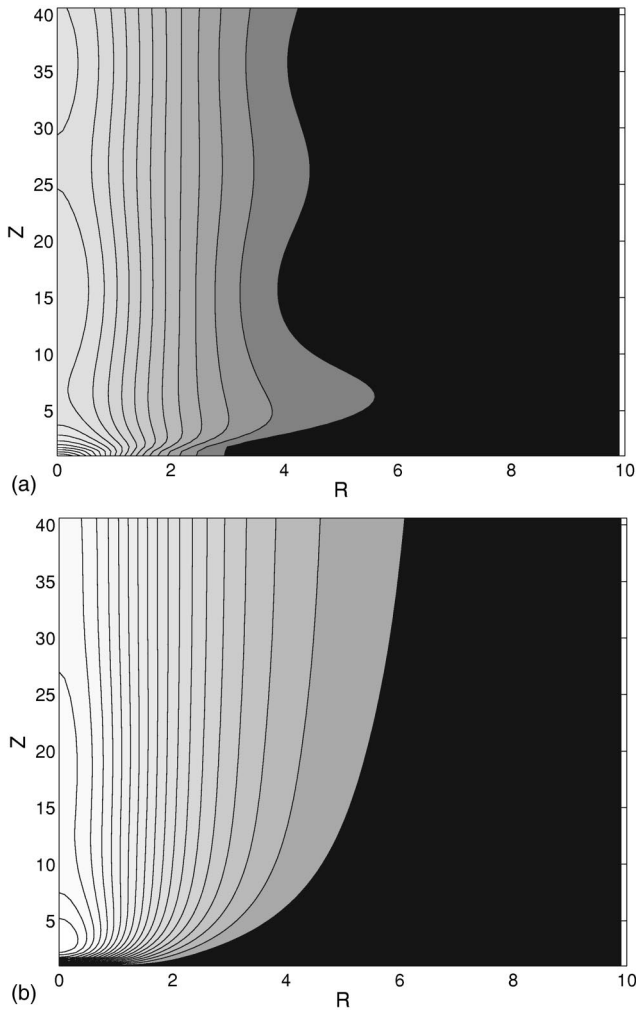


FIG. 6. Contour plot of (a) field amplitude propagation and (b) index modulation evolution in the reduced set (27) for a fiber geometry and  $p=1$ , and with an initial condition for the field given by the self-similar solution and a zero initial index. The brighter areas represent higher values of the field or index.

this to a scaled self-similar solution as before by looking at the maximum values and widths of the field and index modulation. This is achieved by finding the appropriate scaling  $m$  relative to the self-similar solution from Eq. (41) for both the peak value and width. The ratio of these two factors ( $m_{rat} = m_{max}/m_{\rho}$ ) indicates how well the solution matches the self-similar solution. If  $m_{rat} < 1$  the solution is too weak for its width, while if  $m_{rat} > 1$  then it is too strong.

Figure 7 shows the variation of the ratios  $m_{rat}$  for both the field and index modulation as a function of  $Z$ . The initial conditions set the initial values of the ratio for the field to be 1 while that for the index to be zero. The ratio for the index modulation then converges uniformly towards 1 while that for the field remains close to 1 for all times. This indicates that it is possible to join an unexposed section of material with a self-similar waveguide in this case. This result is consistent with the simulations of the full system of PDEs in Fig. 3.

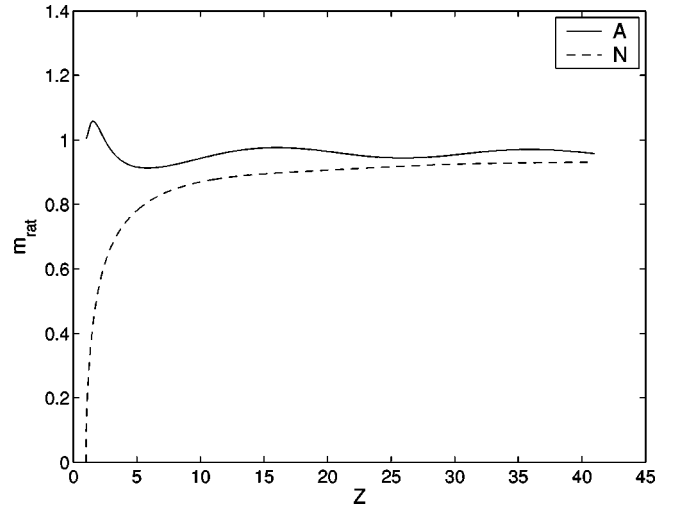


FIG. 7. Ratio of scaling factors as a function of  $Z$  for the field amplitude and the index modulation for fiber geometry and  $p=1$ .

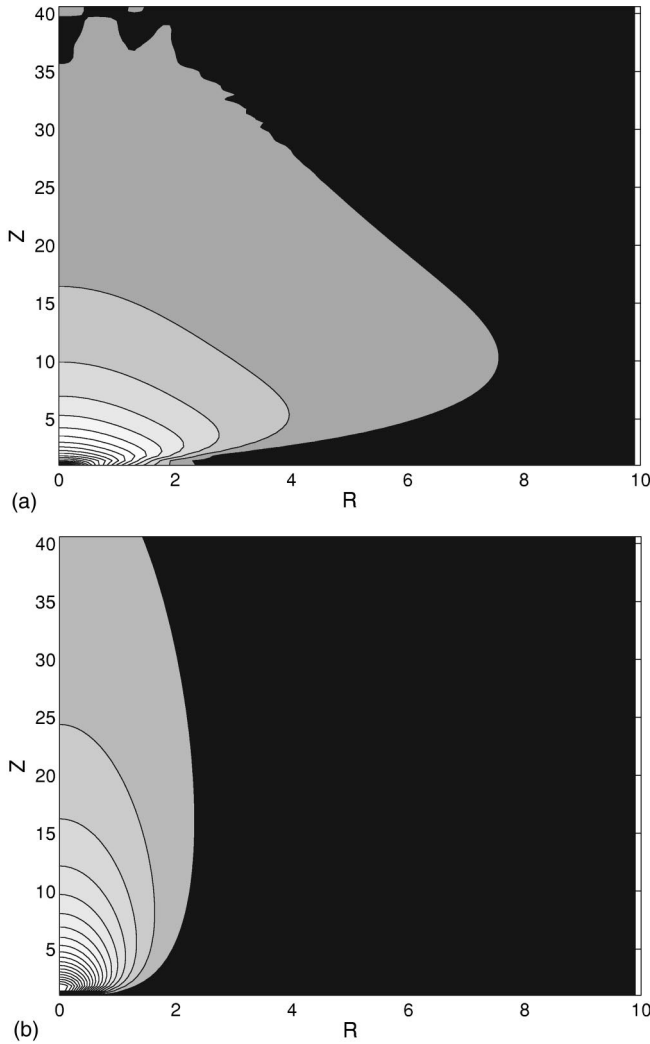
### 2. Fiber geometry— $p=2$

The fiber geometry with  $p=2$  displays a different behavior, as seen in Figs. 8 and 9. No convergence toward a self-similar solution is obvious from the plots, while the values of both ratios remain below 1 at all times after  $Z=0$ . This suggests some kind of instability of the self-similar solution. This result is consistent with the simulations of the full system of PDEs in Fig. 5.

The numerical results presented here are representative of the wide range of input conditions that we have analyzed. The stability of the system for  $p=1$  and instability for  $p=2$  with fiber geometry can be observed as the initial index profile varies over a broad range of strengths relative to the self-similar solution. Equivalent results for the planar geometry are included in Appendix A.

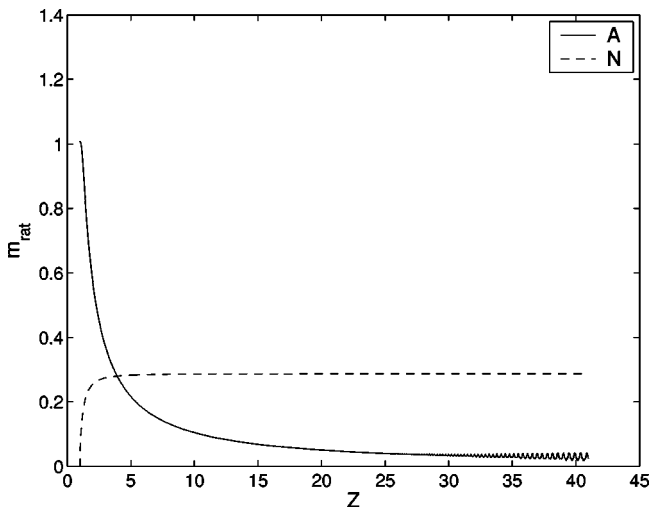
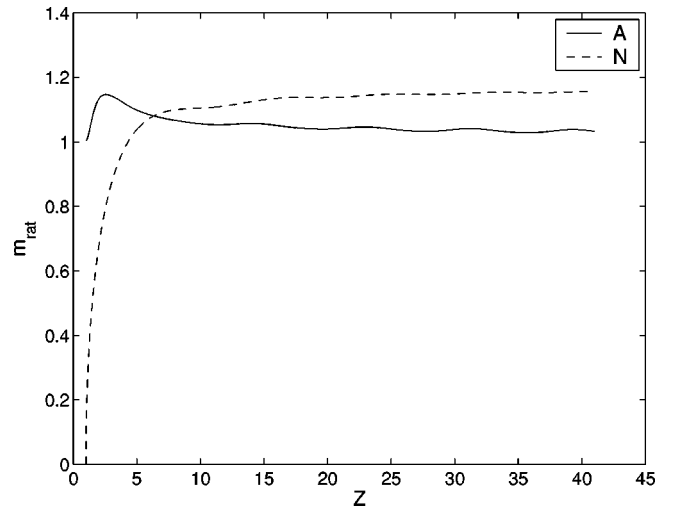
## V. CONCLUSIONS

We have presented a Lie symmetry analysis for the system of equations that describe self-writing in a bulk material. The physical interpretation of the various symmetries are discussed and these have been used to construct similarity-reduced PDEs involving fewer independent variables. The analysis is presented in a general form so that the results are also valid for a planar geometry. We have further reduced the equations to find, to our knowledge, for the first time a class of self-similar modal solutions for bulk materials with a power-law photosensitivity. These solutions are analogous to the self-similar solutions that were previously obtained for the planar case. In contrast to these previous results, however, we find that the self-similar solution in the bulk geometry for  $p=2$  collapses in finite time, and, more generally, that the solutions collapse if  $Dp > 2$ , where  $D$  is the number of transverse dimensions and  $p$  is the order of the photosensitivity process. This collapse appears to be analogous to the collapse of high-dimensional solitons. We also find that for  $p=1$  the self-similar refractive index solution has a  $V$  num-

FIG. 8. As Fig. 6, but for  $p=2$ .

ber that diverges, but that the associated waveguide nonetheless effectively behaves as if it were single mode.

For  $p=1$ , numerical simulations of the full and reduced systems of PDEs are presented that converge to the self-

FIG. 9. As Fig. 7, but for  $p=2$ .FIG. 10. Ratio of scaling factors as a function of  $Z$  for the field amplitude and the index modulation for planar geometry and  $p=1$ .

similar solution for a wide range of initial conditions. These results suggest that the self-similar solution in this case is physically significant and in some sense stable. For  $p=2$ , however, we do not observe such a convergence. This, in addition to the collapse of the self-similar solution for a two-photon process, would suggest that it is physically less interesting.

As mentioned in Sec. II A, saturation of the refractive index change occurs in all physical systems, thus preventing unlimited index growth and collapse. Saturated systems are not described by the most interesting symmetries here, however the results in this paper still provide useful information about the early dynamics of these systems before the onset of saturation and a deeper conceptual understanding of the evolution of self-written structures generally.

#### ACKNOWLEDGMENT

The Australian Research Council supported this work.

#### APPENDIX A: NUMERICAL ANALYSIS OF REDUCED SYSTEM FOR PLANAR GEOMETRY

Previous studies of self-writing in a planar geometry do not include the numerical analysis of the reduced system of PDEs (27). We present the results of some numerical simulations of these equations for  $p=1$  in Fig. 10. As for the simulations presented for the fiber in Sec. IV B the initial condition is given by the self-similar field solution with a zero initial index modulation profile. It is seen that the ratio for the index modulation grows to a value above 1 and remains there. To study this further, we have conducted numerical simulations of the full set of PDEs using the same numerical domain and initial conditions as for the fiber geometry simulations presented in Sec. IV A. Figure 11 shows the index profile at the end face of the simulation scaled to a constant during the evolution of the waveguide. As in Fig. 10, the results reveal an overshoot of the self-written wave-

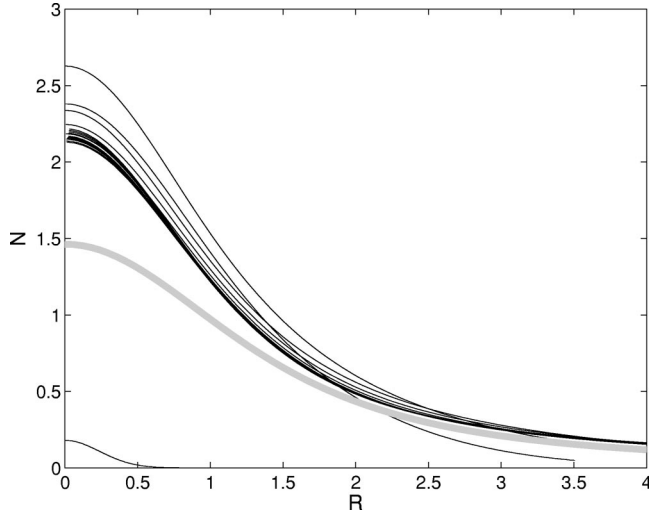


FIG. 11. Similar to Fig. 4, but for a planar geometry.

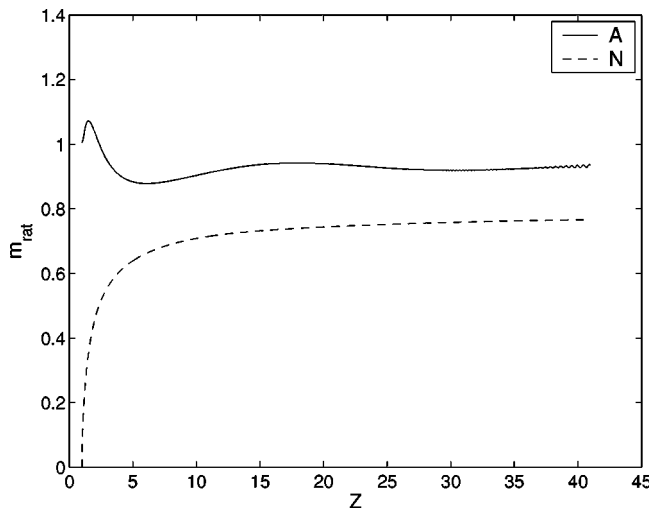
guide compared to the self-similar solution. This overshoot, which is followed by a slow convergence back toward the self-similar solution, was not noticed in previous studies [2,25].

Finally, the simulation for  $p=2$  in Fig. 12 converges slowly towards the self-similar solution, with both values of  $m_{rat}$  approaching 1.

## APPENDIX B: SPECIAL RESULTS FOR $Dp=2$

### 1. Primary Lie symmetry analysis

We start with all the symmetries including the special symmetry in Eq. (19). If we forgo taking advantage of the symmetries associated with  $V_x$ ,  $V_y$ , and  $V_\Theta$  the characteristic equations simplify to


 FIG. 12. Ratio of scaling factors as a function of  $Z$  for the field amplitude and the index modulation for planar geometry and  $p=2$ .

$$\begin{aligned} \frac{dX}{\frac{1}{2}f'(Z)X} &= \frac{dY}{\frac{1}{2}f'(Z)Y} = \frac{dZ}{f(Z)} = \frac{dT}{g(T)} \\ &= \frac{dA}{-\frac{1}{2}\left\{\frac{1}{p}f'(Z)+\dot{g}(T)\right\}A} \\ &= \frac{d\Phi}{\frac{1}{4}f''(Z)R^2+l(Z)+h(T)} \\ &= \frac{dN}{\frac{1}{4}f'''(Z)R^2+l'(Z)-f'(Z)N}. \end{aligned} \quad (\text{B1})$$

Solving the equations we obtain the similarity variables for the three new independent variables

$$\tilde{X} = \frac{1}{\sqrt{f(Z)}}X, \quad (\text{B2a})$$

$$\tilde{Y} = \frac{1}{\sqrt{f(Z)}}Y, \quad (\text{B2b})$$

$$\tilde{Z} = \int^Z \frac{dZ'}{f(Z')} - \int^T \frac{dT'}{g(T')} \quad (\text{B2c})$$

and the transformations for the new dependent variables

$$\tilde{\mathcal{A}}(\tilde{X}, \tilde{Y}, \tilde{Z}) = \sqrt{f(Z)^{1/p}g(T)}\mathcal{A}(X, Y, Z, T), \quad (\text{B2d})$$

$$\tilde{\Phi}(\tilde{X}, \tilde{Y}, \tilde{Z}) = \Phi(X, Y, Z, T) - \varphi(R, Z, T), \quad (\text{B2e})$$

$$\tilde{N}(\tilde{X}, \tilde{Y}, \tilde{Z}) = f(Z)[N(X, Y, Z, T) - \kappa(R, Z)], \quad (\text{B2f})$$

with

$$\varphi(R, Z, T) = \int^Z k(Z')dZ' + \int^T \omega(T')dT' + \gamma(Z)R^2, \quad (\text{B3a})$$

$$\kappa(R, Z) = k(Z) + \{\gamma'(Z) + 2\gamma(Z)^2\}R^2, \quad (\text{B3b})$$

and

$$k(Z) = \frac{l(Z)}{f(Z)}, \omega(T) = \frac{h(T)}{g(T)}, \gamma(Z) = -\frac{f'(Z)}{4f(Z)}. \quad (\text{B4})$$

Using the transformations (B2) and (B3) and reintroducing the complex field  $\tilde{E} = \tilde{\mathcal{A}}e^{i\tilde{\Phi}}$  we obtain the reduced PDEs system involving only three independent variables:

$$i\tilde{E}_{\tilde{Z}} + \frac{1}{2}\tilde{\nabla}_{\perp}^2\tilde{E} + \tilde{N}\tilde{E} = 0, \quad (\text{B5a})$$

$$\tilde{N}_{\tilde{Z}} + |\tilde{E}|^{2p} = 0, \quad (\text{B5b})$$

where  $\tilde{\nabla}_{\perp}^2$  is the transverse Laplacian in the tilde coordinates.

The form of Eqs. (B2) now allows us to interpret the arbitrary functions that appeared initially in the Lie analysis. The function  $f(Z)$  represents arbitrary stretching or scaling of the transverse and longitudinal coordinates, which then also manifests in a rescaling of the amplitude of the field and the refractive index profile. Likewise, the function  $g(T)$  represents arbitrary stretching or scaling of the time coordinates, which also scales the amplitude of the field. The variable  $\tilde{Z}$  can then easily be interpreted as a traveling wave coordinate in the stretched coordinates.

The function  $\varphi$  represents the degree to which the phase of the field is arbitrary and consists of different components. The corresponding wave-vector-like function  $\kappa$  is closely related to the spatial derivative of  $\varphi$  and represents how variations in the phase affect the index profile. The scaling function  $f(Z)$  contributes to a quadratic variation in  $R$  across both the phase front and the index profile through  $\gamma(Z)$ . The arbitrary function  $h(T)$  is proportional to a frequencylike function  $\omega(T)$  which contributes an arbitrary time dependence to the phase of the field through  $\varphi$ . Likewise, the arbitrary function  $l(Z)$  is proportional to a wave-vector-like function  $k(Z)$  which contributes to the arbitrary longitudinal dependence of the phase but also appears as an adjustment to the refractive index profile.

This self-similar solution is quite different from the one in the main body of the paper, since instead of the transverse coordinates scaling with time, they scale with the longitudinal coordinate. Why this type of symmetry should only exist for special values of  $p$  is not clear.

## 2. Secondary Lie symmetry analysis

The reduced PDEs (B5) in three independent variables can be further analyzed for symmetry properties by repeating the Lie analysis. We represent the vector fields using tildes to distinguish them from the vector fields obtained in the first-level analysis. We discover a seven-dimensional subspace of symmetries. The first four are basic coordinate symmetries:

$$\tilde{V}_X = \frac{\partial}{\partial \tilde{X}}, \quad (\text{B6a})$$

$$\tilde{V}_Y = \frac{\partial}{\partial \tilde{Y}}, \quad (\text{B6b})$$

$$\tilde{V}_Z = \frac{\partial}{\partial \tilde{Z}}, \quad (\text{B6c})$$

$$\tilde{V}_\Theta = \tilde{X} \frac{\partial}{\partial \tilde{Y}} - \tilde{Y} \frac{\partial}{\partial \tilde{X}} = \frac{\partial}{\partial \Theta}. \quad (\text{B6d})$$

The next two represent adding an arbitrary constant or a linear function of  $Z$  to the phase. The latter requires simultaneously adding constant to the refractive index:

$$\tilde{V}_\Phi = \frac{\partial}{\partial \Phi}, \quad (\text{B6e})$$

$$\tilde{V}_N = \tilde{Z} \frac{\partial}{\partial \Phi} + \frac{\partial}{\partial \tilde{N}}. \quad (\text{B6f})$$

The final symmetry is a scaling symmetry:

$$\tilde{V}_S = \frac{1}{2} \left( \tilde{X} \frac{\partial}{\partial \tilde{X}} + \tilde{Y} \frac{\partial}{\partial \tilde{Y}} \right) + \tilde{Z} \frac{\partial}{\partial \tilde{Z}} - \tilde{N} \frac{\partial}{\partial \tilde{N}} - \frac{1}{p} \tilde{\mathcal{A}} \frac{\partial}{\partial \tilde{\mathcal{A}}}. \quad (\text{B6g})$$

This last symmetry is the one which we choose to exploit. The invariant surface condition is

$$\frac{d\tilde{X}}{\tilde{X}} = \frac{d\tilde{Y}}{\tilde{Y}} = \frac{d\tilde{Z}}{2\tilde{Z}} = -p \frac{d\tilde{\mathcal{A}}}{2\tilde{\mathcal{A}}} = \frac{d\tilde{\Phi}}{0} = -\frac{d\tilde{N}}{2\tilde{N}}. \quad (\text{B7})$$

A set of similarity variables which are denoted by hats are given by

$$\hat{X} = \tilde{X} / \sqrt{\tilde{Z}}, \quad (\text{B8a})$$

$$\hat{Y} = \tilde{Y} / \sqrt{\tilde{Z}} \quad (\text{B8b})$$

with new dependent variables given by

$$\hat{\mathcal{A}}(\hat{X}, \hat{Y}) = \tilde{Z}^{1/p} \tilde{\mathcal{A}}(\tilde{X}, \tilde{Y}, \tilde{Z}), \quad (\text{B8c})$$

$$\hat{\Phi}(\hat{X}, \hat{Y}) = \tilde{\Phi}(\tilde{X}, \tilde{Y}, \tilde{Z}), \quad (\text{B8d})$$

$$\hat{N}(\hat{X}, \hat{Y}) = \tilde{N}(\tilde{X}, \tilde{Y}, \tilde{Z}). \quad (\text{B8e})$$

The reduced PDE is

$$-\frac{i}{2} (\hat{R} \hat{E}_{\hat{R}} + D \hat{E}) + \frac{1}{2} \hat{\nabla}_{\perp}^2 \hat{E} + \hat{N} \hat{E} = 0, \quad (\text{B9a})$$

$$\frac{1}{2} \hat{R} \hat{N}_{\hat{R}} + \hat{N} - |\hat{E}|^{2p} = 0, \quad (\text{B9b})$$

where  $D$  is the transverse dimensionality of the system and  $\hat{\nabla}_{\perp}^2$  is the transverse Laplacian in the hat coordinates. In two dimensions  $\hat{R} = \sqrt{\hat{X}^2 + \hat{Y}^2}$ , whereas in one dimension  $\hat{R} = \hat{X}$ .

The system can be reduced to an ODE by considering only circularly symmetric solutions leading to

$$-\frac{i}{2} (\hat{R} \hat{E}' + D \hat{E}) + \frac{1}{2} \left( \hat{E}'' + \frac{D-1}{\hat{R}} \hat{E}' \right) + \hat{N} \hat{E} = 0, \quad (\text{B10a})$$

$$\frac{1}{2} \hat{R} \hat{N}' + \hat{N} - |\hat{E}|^{2p} = 0, \quad (\text{B10b})$$

where the prime denotes differentiation with respect to  $\hat{R}$ . We have been unable to find any bound modes of this set of equations using the numerical methods used to find the self-similar solution in Sec. III. We therefore do not study them in detail.

## APPENDIX C: ALTERNATE SIMILARITY VARIABLES

We already discussed how the choice of symmetries that are exploited leads to the different results. However, even from a specific set of invariant surface conditions, the choice of similarity variables is not unique. For example, starting from Eqs. (23) we could have chosen instead variable combinations such as

$$Y/X, \quad (\text{C1a})$$

$$X/(Z-Z_0), \quad (\text{C1b})$$

$$X^2N, \quad (\text{C1c})$$

or indeed any function and combination of the above variables and more. For example,  $\tan^{-1}(Y/X)$  rediscovers the angular coordinate as a similarity variable. A tabulation of all possible similarity variables would be difficult and physically not necessarily productive or illuminating.

- 
- [1] T.M. Monro, D. Moss, M. Bazylenko, C.M. de Sterke, and L. Poladian, *Phys. Rev. Lett.* **80**, 4072 (1998).
- [2] T.M. Monro, C.M. de Sterke, and L. Poladian, *J. Mod. Opt.* **48**, 191 (2001).
- [3] A.A. Sukhorukov, S. Shoji, Yu.S. Kivshar, and S. Kawata, *J. Nonlinear Opt. Phys. Mater.* **11**, 391 (2002).
- [4] C. Meneghini and A. Villeneuve, *J. Opt. Soc. Am. B* **15**, 2946 (1998).
- [5] W.S. Brocklesby, S.J. Field, D.C. Hanna, A.C. Large, J.R. Lincoln, D.P. Shepherd, A.C. Tropper, P.J. Chandler, P.D. Townsend, L. Zhang, X.Q. Feng, and Q. Hu, *Opt. Mater. (Amsterdam, Neth.)* **1**, 177 (1992).
- [6] A.S. Kewitsch and A. Yariv, *Opt. Lett.* **21**, 24 (1996).
- [7] A.S. Kewitsch and A. Yariv, *Appl. Phys. Lett.* **68**, 455 (1996).
- [8] S. Shoji and S. Kawata, *Appl. Phys. Lett.* **75**, 737 (1999).
- [9] S.J. Frisken, *Opt. Lett.* **18**, 1035 (1993).
- [10] D. Homoelle, S. Wielandy, A.L. Gaeta, N.F. Borrelli, and C. Smith, *Opt. Lett.* **24**, 1311 (1999).
- [11] G.I. Stegeman and M. Segev, *Science* **286**, 1518 (1999).
- [12] S. Shoji, S. Kawata, A.A. Sukhorukov, and Y.S. Kivshar, *Opt. Lett.* **27**, 185 (2002).
- [13] A.M. Ljungström and T.M. Monro, *J. Lightwave Technol.* **20**, 78 (2002).
- [14] A.M. Ljungström and T.M. Monro, *Opt. Express* **10**, 230 (2002).
- [15] M. Senthilvelan, L. Poladian, and C.M. de Sterke, *Phys. Rev. E* **65**, 066607 (2002).
- [16] J. Weiss, M. Tabor, and G. Carnevale, *J. Math. Phys.* **24**, 522 (1983).
- [17] M.J. Ablowitz and P.A. Clarkson, *Solitons, Nonlinear Evolution Equations and Inverse Scattering Transform* (Cambridge University Press, Cambridge, 1990).
- [18] P.J. Olver, *Applications of Lie Groups to Differential Equations* (Springer, New York, 1986).
- [19] G.W. Bluman and S. Kumei, *Symmetries and Differential Equations* (Springer, New York, 1989).
- [20] S. An and J.E. Sipe, *Opt. Lett.* **16**, 1478 (1991).
- [21] C.R. Menyuk, D. Levi, and P. Winternitz, *Phys. Rev. Lett.* **69**, 30 488 (1992).
- [22] M.E. Fermann, V.I. Kruglov, B.C. Thomsen, J.M. Dudley, and J.D. Harvey, *Phys. Rev. Lett.* **84**, 6010 (2000).
- [23] A. Head, *Comput. Phys. Commun.* **77**, 241 (1993).
- [24] G. Baumann, *Symmetry Analysis of Differential Equations with Mathematica* (Springer, New York, 2000).
- [25] T.M. Monro, P.D. Miller, L. Poladian, and C.M. de Sterke, *Opt. Lett.* **23**, 268 (1998).
- [26] S. Wolfram, *The Mathematica Book*, 5th ed. (Wolfram Media/Cambridge University Press, Cambridge, 2003).
- [27] A.W. Snyder and J.D. Love, *Optical Waveguide Theory* (Chapman and Hall, London, 1983).